frontiers | Frontiers in Earth Science

TYPE Original Research
PUBLISHED 07 October 2024
DOI 10.3389/feart.2024.1401066

Check for updates

OPEN ACCESS

EDITED BY
Bayasgalan Amgalan,
IAG, Mongolia

REVIEWED BY
Liang Qiu,
China University of Geosciences, China
Chih-Tung Chen,
National Central University, Taiwan

*CORRESPONDENCE
Qingyun Zhou,
zhouqingyun@pku.edu.cn

RECEIVED 14 March 2024
ACCEPTED 24 September 2024
PUBLISHED 07 October 2024

CITATION
Zhou Q (2024) Clockwise extrusion of the Sichuan-Yunnan block toward the Red River Fault in the southeastern Tibetan Plateau. *Front. Earth Sci.* 12:1401066.
doi: 10.3389/feart.2024.1401066

COPYRIGHT
© 2024 Zhou. This is an open-access article distributed under the terms of the Creative Commons Attribution License (CC BY). The use, distribution or reproduction in other forums is permitted, provided the original author(s) and the copyright owner(s) are credited and that the original publication in this journal is cited, in accordance with accepted academic practice. No use, distribution or reproduction is permitted which does not comply with these terms.

Clockwise extrusion of the Sichuan-Yunnan block toward the Red River Fault in the southeastern Tibetan Plateau

Qingyun Zhou[1,2]*

[1]Yunnan Earthquake Agency, Kunming, Yunnan, China, [2]Kunming Institute of Earthquake Forecast, China Earthquake Administration, Kunming, Yunnan, China

The Xiaojiang Fault and the Red River Fault, which are located on the southeastern margin of the Tibetan Plateau, are the eastern and southern boundaries of the Sichuan–Yunnan Block, respectively. The relationship between these two faults is highly important for the study on the tectonic evolution and seismic risk of the southeastern margin of the Tibetan Plateau. Using the digital elevation model (DEM) data, we extracted and analyzed the maximum elevation, peak steepness index, maximum slope, and relatively flat surface of the Ailaoshan Shear Zone on the southwest side of the Red River Fault. The results revealed that the geomorphic indices result around Yuanjiang were significantly lower than those on the northern and southern sides of Yuanjiang. On the basis of lithology, climate and tectonics, it is inferred that tectonic activity is the main factor controlling landform development. On the basis of existing geophysical and geomorphic survey results in this area, a geodynamic model of this area was constructed: in the mid-Miocene, tectonic inversion of the Red River Fault occurred, and material from the Tibetan Plateau flowed into the Sichuan-Yunnan Block around the East Himalayan Syntax. The resulting extrusion caused the Red River Fault to bend of ~50 km; in the early Pliocene, the middle and lower crust broke through the barrier and entered the interior of the Ailaoshan Shear Zone. Because of the extrusion of the middle and lower crust, the role of the Red River Fault as the boundary has weakened.

KEYWORDS

Red River Fault, Xiaojiang Fault, geodynamic model, geomorphic parameters, extrusion process, southeastern margin of the Tibetan Plateau

1 Introduction

The southeastern margin of the Tibetan Plateau is located on the southeast side of the East Himalaya Syntax (EHS) and has experienced strong lateral extrusion and deformation in the Cenozoic (Molnar and Tapponnier, 1975; Yin and Harrison, 2000; Schoenbohm et al., 2006; Liu-Zeng et al., 2008; Xu et al., 2011a; Zhao et al., 2023; Zhang et al., 2023). Studying the deformation model of the southeastern margin of the Tibetan Plateau is particularly important for understanding the tectonic evolution and uplift of the plateau (Wang et al., 1998; Burchfiel and Chen, 2012; Deng et al., 2014). Scholars have conducted extensive geological and geomorphic mapping, including chronological analysis, geodetic surveying, geophysical observation, and geodynamic

simulation, over the past half-century in this area, enabling us to understand the tectonic evolution and dynamic processes (Molnar and Tapponnier, 1975; Peltzer and Tapponnier, 1988; Royden et al., 1997; Flesch et al., 2001; Replumaz and Tapponnier, 2003; Copley, 2008; Wen et al., 2011; Shi et al., 2018). On the basis of GPS data, researchers generally agree that the crust and mantle on the southeastern margin of the Tibetan Plateau have rotated clockwise around the EHS (Wang and Shen, 2020; Gan et al., 2022).

The two most important tectonic systems along the southeastern margin of the Tibetan Plateau are the Xiaojiang Fault and the Red River Fault systems. The Red River Fault is an old deep fault that has played an important role in the three stages of deformation of the southeastern margin of the Tibetan Plateau (Shi et al., 2018; Guo et al., 1996; Li et al., 2016b; Ye et al., 2022; Zhou et al., 2023). The Xiaojiang Fault, which formed in the middle and late Miocene, is the eastern boundary of the clockwise rotation area, as well as the boundary between the South China Block and the Sichuan–Yunnan Block (Wen et al., 2011; Ren, 2013; Han et al., 2017). The relationship between these two faults is significant for our study of tectonic evolution and the seismic risk along faults. If the Xiaojiang Fault cuts the Red River Fault, then the seismic risk in the southern segment of the Red River Fault (southern to the cutting point) decreases; otherwise, the southern segment of the Red River Fault has a greater seismic risk. Some researchers believe that the Xiaojiang Fault terminates north of the Red River Fault; that is, the Xiaojiang Fault does not cut through the Red River Fault. Throughout the whole tectonic history, the Red River Fault has maintained a dominant role (Wen et al., 2011; Li and Wang, 1975; Tapponnier et al., 1982; He et al., 1992; Roger et al., 1995; Song and Wang, 1998; Replumaz et al., 2001; Xu et al., 2003; Zhang et al., 2003; Xu et al., 2011b). Other researchers believe that the Xiaojiang Fault has shifted to the left, crossed the Red River Fault and played a dominant role in the tectonic evolution. Moreover, the northern segment of the Red River Fault has become a secondary fault, and the southern segment is less dangerous (Schoenbohm et al., 2006; Wang et al., 1998; Lacassin et al., 1998; Chen et al., 2000; Schoenbohm et al., 2004; Shen et al., 2005; Simons et al., 2007; Wu et al., 2015; Zhang and Ding, 2016; Dong et al., 2023). Therefore, determining the relationship between the Red River Fault and the Xiaojiang Fault is the key basis for obtaining geodynamic models of the region and is the purpose of this research.

Many researchers have carried out research in the area of the intersection of the Red River Fault and the Xiaojiang Fault. Li and Gao (2023) obtained the direction of fast waves of crustal shear wave splitting data under a survey line. On the basis of the distribution of fast crustal shear waves, the directions of fast waves on the west side and east side of the Yuanmou Fault are nearly orthogonal. According to seismic waveform analysis (Li et al., 2020) and Interferometric Synthetic Aperture Radar (InSAR) coseismic deformation studies (Sun and Liu, 2019), the seismic fault of the Yuanjiang Ms5.9 earthquake on 8 September 2018, should have been a concealed fault in the northeast. Seismic wave velocity tomography results, including those of deep seismic reflections (Zhang, et al., 2013), body waves and surface waves (Liu et al., 2023; Wang et al., 2024), also indicate that this area has a complex tectonic background. The above data suggest that the crust on the west side of the Xiaojiang Fault may have crossed the Red River Fault, but all this evidence is only secondary evidence or even tertiary evidence. We still need more convincing evidence.

According to the results of geophysical exploration, there are differences in the P-wave velocities of the crust on both sides of the Red River Fault, which are related to the difference in the density of the material on the two sides (Bai and Wang, 2004; Zhang et al., 2013). The clockwise rotation of the GPS data reflects the clockwise flow of crust and mantle (Wang and Shen, 2020; Gan et al., 2022). If it is proven that the crust and mantle of the Sichuan-Yunnan Block entered the Shan-Thai Block through the Red River Fault, it may also be correct that the Xiaojiang Fault intersects the Red River Fault. The Ailaoshan Shear Zone was divided into three segments (the northern, middle and southern segments in Figure 1), and the geomorphological characteristics of the three segments were studied. On the basis of the results of this study and geophysical and geomorphic data, we discuss whether the crust of the Sichuan–Yunnan Block crossed the Red River Fault and entered the Ailaoshan Shear Zone; thus, the intersection between the Xiaojiang Fault and the Red River Fault may be determined.

2 Geologic setting

The Red River Fault is the southwestern boundary of the Sichuan–Yunnan Block. The southern segment of the Red River Fault is also the boundary between the South China Block and the Shan Thai Block (Qiu et al., 2016; Yang et al., 2021; Zhang et al., 2023). The fault starts in Eryuan County, Yunnan Province, in the northwest, is located approximately along the Red River valley and extends southeast to the South China Sea, with a total length of more than 1,000 km. The overall strike of the fault ranges from 310° to 320°, and the strike of the area of intersection with the Xiaojiang Fault changes to 290°–300°, revealing a concave turn (Tapponnier, et al., 1990; Leloup et al., 1995; 2007; Guo et al., 1996; Li et al., 2016b; Shi et al., 2018; Ye et al., 2022; Zhou et al., 2023). The Red River Fault served an important role in three stages (crustal shortening and thickening in the Eocene, lateral extrusion of blocks in the Oligocene, and tectonic inversion in the Miocene–Pliocene) of the Cenozoic tectonic evolution of the southeastern margin of the Tibetan Plateau. It has played an important role in tectonic evolution (Wang et al., 2022). Historically, 3M ≥ 7 earthquakes occurred on the Red River Fault. These three earthquakes all occurred within 120 km of the northernmost end of the fault (north of Juli). There is no historical record of an earthquake with a magnitude greater than 7 in southern Juli. Therefore, the northern segment of the Red River Fault is generally considered a Holocene fault, and the periods in which activity occurred in the central and southern segments need to be studied further. The Red River Fault has not been very well studied, and many aspects need further work, for example, whether the Xiaojiang Fault crosses the Red River Fault and why all trenches along the middle valley fault have not revealed a significant dip-slip component (Allen et al., 1984; Shi et al., 2018; Li et al., 2016b; Shi et al., 2018; Zhou et al., 2023).

The Xiaojiang Fault is the eastern boundary of the Sichuan-Yunnan Block, and it is also the eastern boundary fault of the southeastern margin of the Tibetan Plateau that rotates clockwise (Wen et al., 2011; Ren, 2013; Han et al., 2017). The northern end of the fault connects to the Zemuhe Fault, and

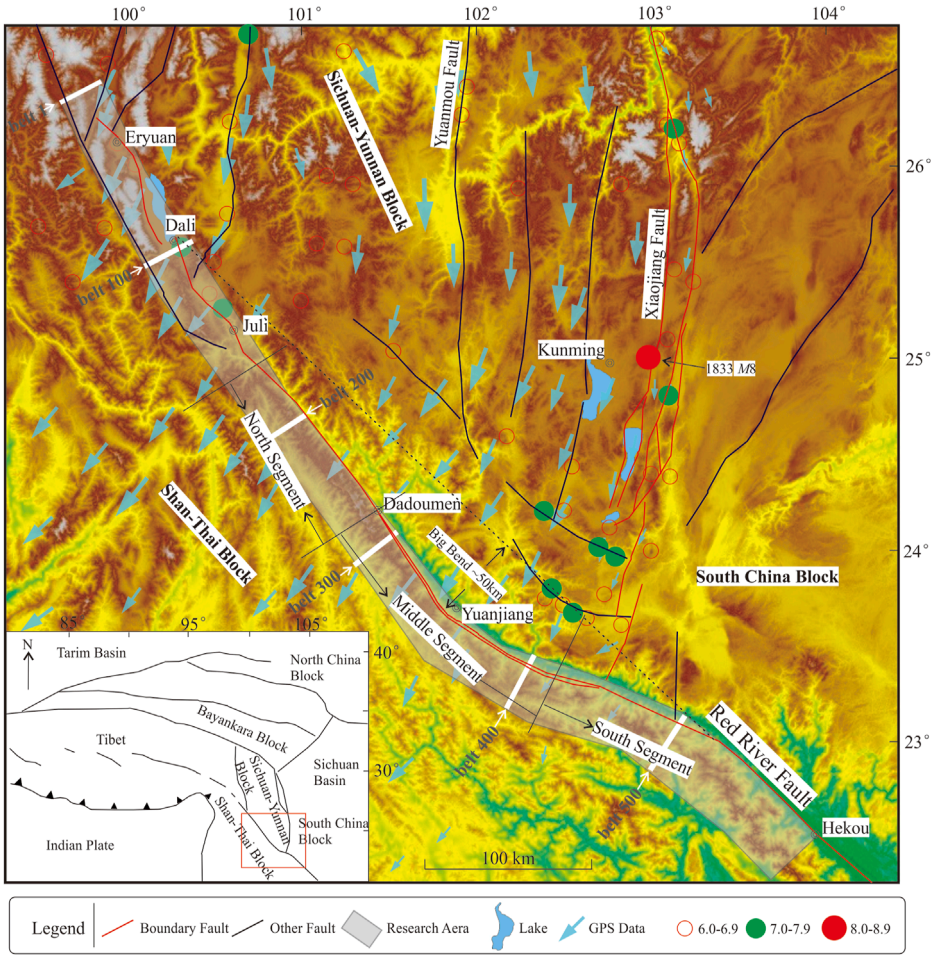

FIGURE 1
Geographic map of the southeastern Tibetan Plateau area and study region. The GPS data applied in this figure were obtained from Wang and Shen (2020). The GPS velocity field is relative to the stable South China Block. The northern, middle and southern segments jointly constitute the Ailaoshan Shear Zone (ASZ).

the southern end, according to large-scale geological mapping, extends to the vicinity of the Red River Fault (Wen et al., 2011; Guo et al., 2021). The Xiaojiang Fault is the most active fault on the southeastern margin of the Tibetan Plateau, and its sinistral strike-slip rate reaches 8–10 mm/a (Song and Wang, 1998; Hu et al., 2023). The Xiaojiang Fault is a nascent active fault that formed after the Miocene–Pliocene tectonic inversion. Historically, several earthquakes with magnitudes greater than 7 that occurred on the Xiaojiang Fault have been recorded. The largest historical earthquake, the Songming M8 earthquake, in Yunnan, also occurred on the Xiaojiang Fault (Yu et al., 2022). It is also a deep fault that cuts through the crust.

The Ailaoshan–Red River Shear Zone is considered to constitute the northeastern boundary of the Shan-Thai Block. This shear zone starts in Weixi County, Yunnan Province, in the north, passes through Vietnam and then enters the South China Sea in the southeast, with a total length of more than 1,000 km. From northwest to southeast, this shear zone is composed of the Xuelongshan Shear Zone, Diancangshan Shear Zone, Ailaoshan Shear Zone and Daxiangshan Shear Zone (Wang et al., 2022). The study area in this paper is the Ailaoshan Shear Zone. The Ailaoshan Shear Zone starts from Midu in the north and extends southeastward via Yuanjiang, Yuanyang and Laojie into Vietnam. The Ailaoshan Shear Zone is mainly composed of a low greenschist facies zone (schist, slate, metamorphic sandstone, etc.) and a high greenschist–amphibolite facies belt (including mylonite, gneiss, migmatite, plagioclase, amphibolite, etc.) (Leloup et al., 1995; 2001; Yunnan Bureau of Geology and Mineral Resources, 1990; Zhang et al., 2006; Liu et al., 2012).

3 Data and methods

We used the 30-m resolution DEM dataset downloaded from the United States Geological Survey (USGS). This dataset is based on the National Aeronautic and Space Administration (NASA)'s Shuttle Radar Topography Mission (SRTM) satellite data. The SRTM satellite was launched in 2000 at a flight altitude of approximately 233 km and covers the area from 60° north of the equator to 56° south of the equator. The SRTM satellite is equipped with a synthetic

aperture radar (SAR) instrument, which can use a radar beam to detect the Earth's surface and obtain high-precision surface elevation information. The resolution of the data was 30 m; that is, the ground area represented by each pixel was 30 m × 30 m. This dataset was generated with the World Geodetic System 1984 (WGS84) spatial reference system. This dataset is free to download from the USGS website, which also provides functions such as web services and map browsers.

Spatially, we used data from the Red River Fault, which is approximately 30 km wide in the southwest direction (Figure 1). The main geological tectonic unit in the study area is the Ailaoshan Shear Zone. We divided the DEM of the Ailaoshan Shear Zone into 700 rectangles (or approximately rectangular trapezoids; the range is the shaded part in Figure 1) with a width of 1 km. The long sides of these rectangles are basically perpendicular to the Red River Fault. We marked the locations of some belts in Figure 1 (e.g., belt 1, belt 100, and belt 200). The DEM data were converted to text files via MATLAB, and then, statistical analysis was performed on the elevation data in each rectangle.

In previous geomorphological studies on active tectonics, scholars tended to use geomorphic indicators, especially river geomorphic indicators, such as the hypsometric integral (HI), channel steepness index (*ksn*), and basin shape index (BS), to describe the level of tectonic activity (Horton, 1945; Strahler, 1950; Kirby et al., 2003; Lidmar-Bergström, 1996; Zhang et al., 2008; Jotheri et al., 2019; 2022; Zhao et al., 2023). These parameters can quantitatively reflect the relationship between geomorphic evolution and tectonic uplift; therefore, they have been widely used in neotectonic studies. The focus of this paper is not the activity level of each segment of the Red River Fault but rather the traces of tectonic movement perpendicular to the direction of the Red River Fault (the direction of the strike of the Xiaojiang Fault). No river has formed in this direction, and the spatial scale is relatively small; thus, the present study used another geomorphic indicator.

3.1 Maximum elevation (ME_n)

The highest point on the topography reflected the original height of the planation surface (or quasiplain, erosion surface, denudation surface, etc., which was not differentiated in this paper) (Millán et al., 1995; Widdowson, 1997; Liu et al., 2006). During the three Cenozoic evolutionary stages of the southeastern margin of the Tibetan Plateau, no large geological tectonic unit crossed the Ailaoshan Shear Zone. Moreover, active tectonic geomorphology and paleoseismology have shown no evidence of vertical slip along the Red River Fault within the range of the Ailaoshan Shear Zone, and low-temperature thermochronological data also provide no clear evidence that there was significant differential uplift in the various segments of the Ailaoshan Shear Zone (Tapponnier et al., 1990; Leloup et al., 1995; 2001; Wang et al., 2022; Wang et al., 2016; 2020). Therefore, the highest points of each segment of the Ailaoshan Shear Zone should be approximately at the same height or should exhibit a linear trend. The significant change in elevation at the highest point may be related to tectonic activity. Since certain errors in the DEM data exist, the maximum elevation in the belt cannot be simply selected as the resultant maximum elevation (ME). Instead, the arithmetic mean of the values of the highest n point (ME_n) is used to represent the maximum elevation. The formula for calculating the ME_n is as follows (Equation 1):

$$ME_n = \sum_{i=1}^{n} H_i/n \quad (1)$$

where Hi refers to the *i*-th highest point in the strip.

3.2 Peak steepness index (PSI_n)

In general, during tectonic movement, under the same conditions, relatively uplifted areas experience greater erosion, and the resulting mountain peaks become steeper. By studying the steepness indices of mountain peaks in different belts, the relative uplift area and the relative subsidence area can be identified. Some geomorphic indicators are close to the PSI_n, such as the relief degree of the land surface (RDLS) (e.g., Finlayson, 2013; Hamdouni et al., 2008). The method for calculating the RDLS is used to calculate the difference between the highest altitude and the lowest altitude in a certain area. Owing to the existence of deep Red River valleys, RDLS is not suitable for the study area. In this study, the formula for calculating PSI_n is as follows (Equation 2):

$$PSI_n = H_1\text{-}H_n \quad (2)$$

where H_1 refers to the point with the highest altitude in the belt and H_n refers to the point with the n-th highest altitude in the belt. When n is maximized, the meaning of PSI_n is consistent with that of RDLS.

3.3 Maximum slope (MS_n)

Slope is one of the traditional indicators in terrain analysis (Schmidt and Montgomery, 1995; Whipple et al., 1999; Whipple and Tucker, 1999). The slope refers to the slope angle of the ground and can generally be obtained from DEM data through the relationship between the grid point and eight adjacent points (called the D8 algorithm). The slope reflects the intensity of erosion, and the intensity of erosion is related to uplift or a decrease in tectonic activity. The maximum rate of change in elevation (Burrough and Mcdonnell, 1998) between each cell was used to calculate the slope. Similarly, owing to the possibility of certain errors in the DEM data, we generally chose the values of the first n data points as the arithmetic means to represent the maximum slope within the area. The formula for calculating the MS_n is as follows (Equation 3):

$$MS_n = \sum_{i=1}^{n} S_i/n \quad (3)$$

where S_i refers to the *i*-th point in the strip with the largest slope.

3.4 Relatively flat surface (elevation-frequency statistics)

The release and free acquisition of high-precision DEM data have prompted many scholars to develop a variety of methods to identify the planation surface (or erosion surface) based on DEM data and ArcGIS technology (Macmillan et al., 2000; Qian et al.,

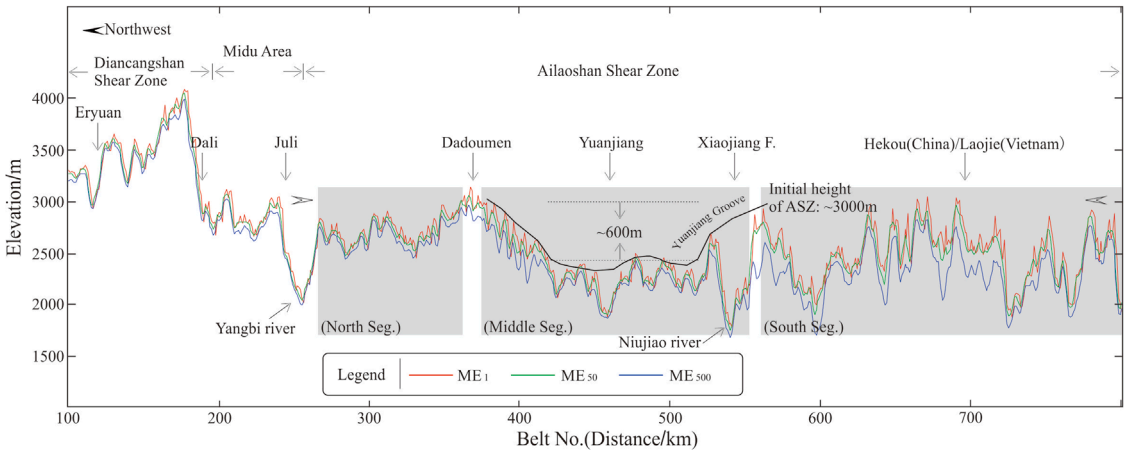

FIGURE 2
Maximum elevation results along the Red River Fault (3-point smoothing). ME_1, ME_{50} and ME_{500} indicate the mean values of the altitudes of the 1, 50 and 500 points, respectively, with the highest altitude in each strip. The shaded area indicates the northern, middle and southern sections of the Ailaoshan Shear Zone. The ME_n near Yuanjiang (belts 320–420) was significantly lower than that in the northern and southern sections; we named this area the "Yuanjiang Groove".

2016). These methods may have poor applicability in our study area for two reasons. First, the erosion in the study area was particularly strong, making it difficult to find a relatively flat surface. Second, the study area was small. Therefore, in this study, the elevation-frequency statistics method was used to identify possible flat surfaces. We compared our calculated results with the results of the field survey to prove the reliability of this method.

The elevation frequency statistics were as follows: (1) the study area was divided into three statistical areas: the northern statistical area, middle statistical area, and southern statistical area (corresponding to the northern segment, middle segment and southern segment of the Red River Fault); (2) in each statistical area, the frequency of all elevations was determined; and (3) the statistical results were drawn in an image to identify points with particularly high frequency. The elevation corresponding to this point is the elevation of the relatively flat surface.

4 Results

4.1 Maximum elevation (ME_n)

Figure 2 shows the highest value (MN_1), the mean value of the highest 50 points (MN_{50}) and the mean value of the highest 500 points (MN_{500}) for each band, and the three curves were consistent. The results revealed that (1) the highest elevation of each segment of the Ailaoshan Shear Zone was approximately 3,000 m; (2) the topography of the southern section of the Ailaoshan Shear Zone was relatively large, indicating that this area has experienced strong erosion; and (3) there was a "U-shaped" groove (called the Yuanjiang Groove) in the middle segment of the Ailaoshan Shear Zone (from 320 to 420 km), which means that subsidence occurred there. The amplitude of the subsidence was approximately 600 m, and the length of the subsidence area was approximately 100 km.

4.2 Peak steepness index (PSI_n)

Figure 3 shows the results for the PSI_{200}, PSI_{1000} and PSI_{3000}. The three indices (Figures 3A–C) exhibited similar characteristics. Specifically, the PSI_n at the northern end of the Ailaoshan Shear Zone was low and similar to that in the Eryuan and Dali areas to the north, indicating that in the Ailaoshan Shear Zone, the PSI_n gradually increased from north to south, mainly because the altitude of the Red River decreased from 2000 m to 100 m. Similarly, in the middle section of the Ailaoshan Shear Zone, a significant low-value anomaly appeared at 320–420 km (Yuanjiang Groove); the PSI_{200} was 300–400 m lower than the expected value, the PSI_{1000} was 400–700 m lower than the expected value, and the PSI_{3000} was 700–900 m lower than the expected value.

4.3 Maximum slope (MS_n)

The MS_{200}, MS_{1000} and MS_{3000} results are shown in Figures 4A–C. In the range of 320–420 km, the slope was 2°–5° lower than that on the northwest side and 6°–14° lower than that on the southeast section, revealing a less obvious groove overall. Compared with the ME_n and PSI_n, the MS_n did not describe the Yuanjiang groove well.

We counted the frequency of slope values among the three segments of the Ailaoshan Shear Zone (Figure 4D). The maximum slope in the middle segment of the Ailaoshan Shear Zone was approximately 61°–62°, and the extrapolated maximum may be approximately 63° (green dotted line in Figure 4D); the maximum slope in the northern segment was approximately 66°–67° (red dotted line in Figure 4D), and the maximum extrapolation may be approximately 78°; the maximum slope in the southern section was approximately 75°, and the extrapolated maximum was approximately 86° (blue dotted line in Figure 4D). An obvious low-slope groove formed in the middle segment of the Ailaoshan Shear Zone. The slopes of the fitting lines in the southern section and

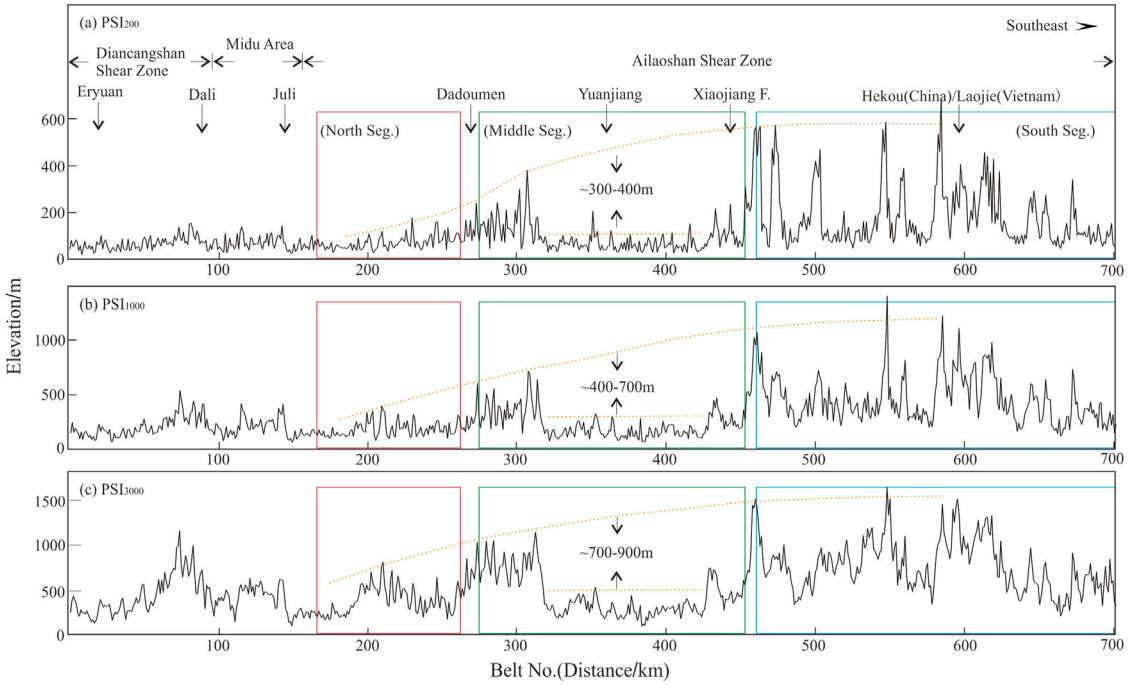

FIGURE 3
Peak steepness index results along the Red River Fault. The **(A)** PSI_{200}, **(B)** PSI_{1000}, **(C)** PSI_{3000} indicate the average values of the slopes of 200, 1,000 and 3,000 points, respectively, with the highest peak steepness index in each strip. The red, green and blue rectangles indicate the northern, middle and southern segments of the Ailaoshan Shear Zone, respectively. The PSI_n near Yuanjiang (belts 320–420) was significantly lower than that in the northern and southern segments, indicating that the erosion in this area was weaker and that the mountain peaks were not steep.

the northern section were very close, indicating that the erosive environments in the southern section and the northern section were similar. Accordingly, it is speculated that the middle section also experienced a similar erosional environment if there was no tectonic movement. At present, the slope of the fitting line in the middle segment is significantly different from that in the southern and northern segments, indicating that the erosional environment in this segment was inconsistent with that in the northern and southern segments.

4.4 Relatively flat surface (elevation frequency statistics)

Figure 5 shows the elevation-frequency diagram of the three segments of the Ailaoshan Shear Zone. In Figure 5, the area above 1,000 m on the blue line is a straight line, indicating that there is basically no smooth surface in the southern segment of the Ailaoshan Shear Zone. The erosion in the northern and middle segments of the Ailaoshan Shear Zone was slightly weaker than that in the southern segment, and the high-elevation sections still had relatively slightly flatter slopes. On the basis of the elevation-frequency map (Figure 5), we identified two relatively flat slope surfaces, namely, flat surface 1 and flat surface 2, in the high-altitude areas of the northern and middle sections of the Ailaoshan Shear Zone. Since the morphological heights of the green line at 1700–2,500 m and the red line at 2,500–3,000 m are highly similar, we speculate that FS1 in the northern section and FS1 in the middle section may be on the same plane, as are FS2 in the northern section and FS2 in the middle section. According to the analysis of the altitudes of the northern and middle sections of FS1 and FS2, the elevation of the middle section of FS1 decreased by 500–600 m, and that of FS2 decreased by 700–800 m. There are two prominent high points in FS2 in the middle segment of the Ailaoshan Shear Zone and two slightly high points in FS2 in the southern segment of the Ailaoshan Shear Zone. If they were located on the same plane and had a one-to-one correspondence, then the decline in the middle section would be 676–718 m.

5 Discussion

5.1 Influences of nontectonic factors

In terms of lithology, the Ailaoshan Shear Zone is mainly composed of rocks such as schist, slate, gneiss, mélange, and plagioclase-rich rocks (http://ngac.org.cn/onemap/index.html) (Leloup et al., 1995; 2001; Zhang et al., 2006; Liu et al., 2012). According to the geological map (Figure 6) (Figure R3), the rocks in the northern section are mainly Proterozoic (Pta), followed by Permian (P) and Silurian (S) in age; the rocks in the middle section are mainly Proterozoic (Pta), followed by Silurian (S) and Triassic (T) in age; and the rocks in the southern section are mainly Proterozoic (Pta), followed by Triassic (T) and Ordovician (O) in age. The distributions of these rocks have the following characteristics. First, the three segments of the Ailaoshan Shear

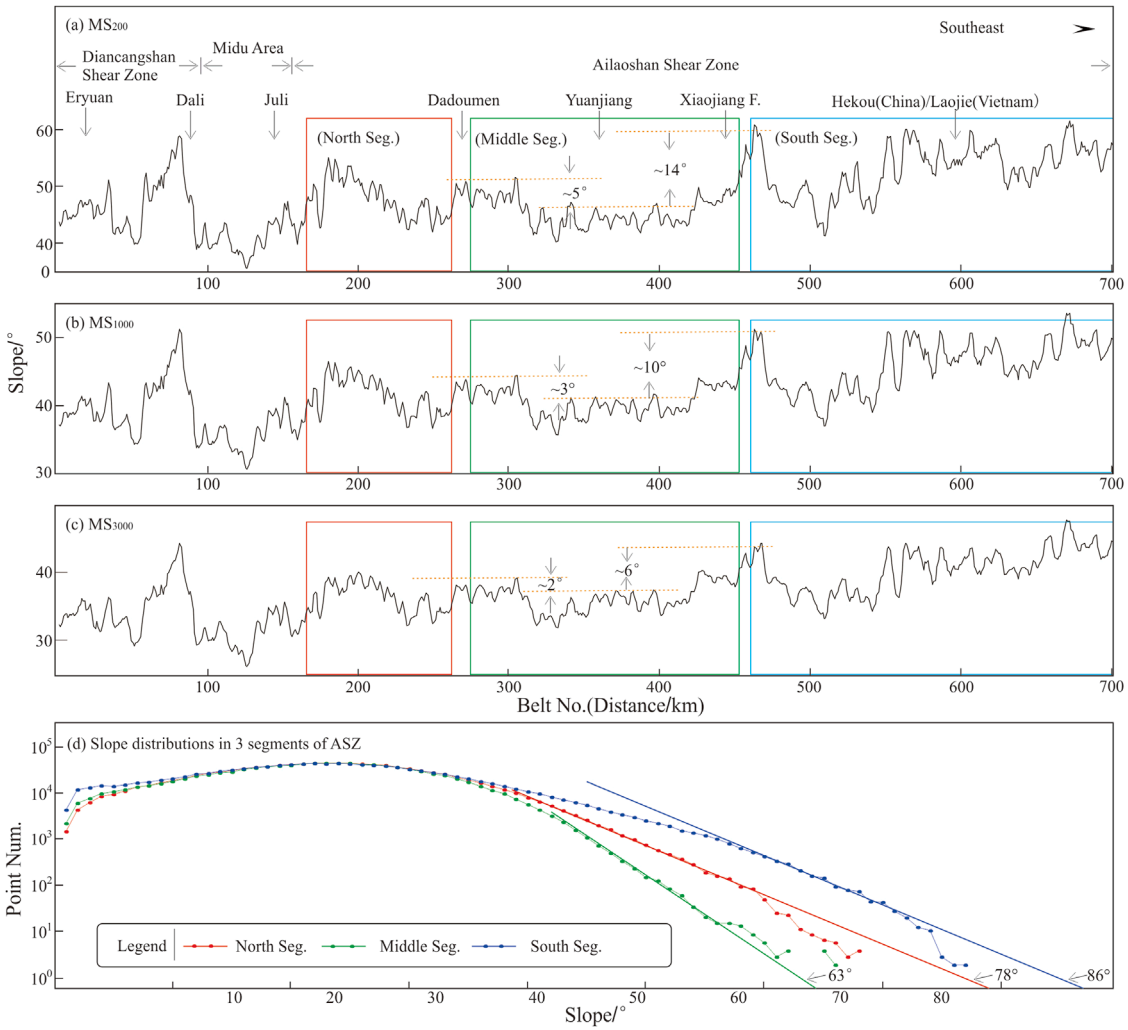

FIGURE 4
(A–C) Maximum slopes along the Red River Fault. The MS_{200}, $MS_{1000}$and MS_{3000}indicate the mean values of the altitudes of the 200, 1,000 and 3,000 points, respectively, with the maximum slope in each strip. The red, green and blue rectangles indicate the northern, middle and southern segments of the Ailaoshan Shear Zone, respectively. **(D)** Frequencies of slope values among the three segments of the Ailaoshan Shear Zone.

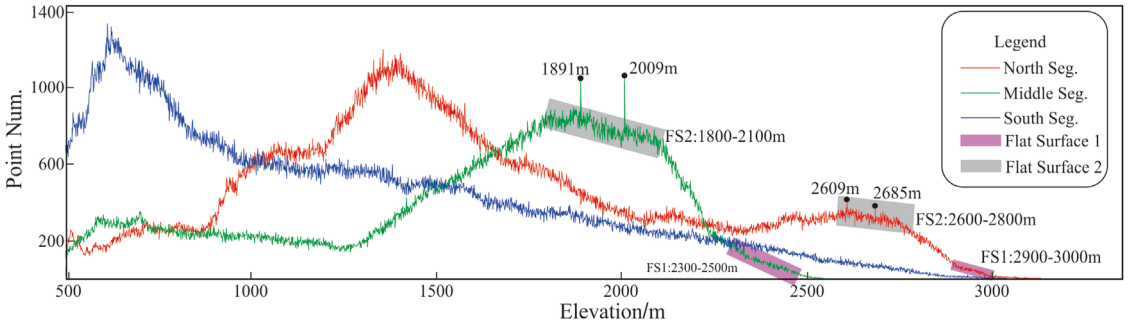

FIGURE 5
Elevation–frequency map of the three segments of the Ailaoshan Shear Zone. The rectangular boxes indicate possible relatively flat slopes. On the basis of the high similarity in shape between the red line at 1700–2,500 m and the green line at 2,500–3,000 m, FS1 in the northern section and FS1 in the middle section may be in the same plane, and FS2 in the northern section and FS2 in the middle section may also be in the same plane.

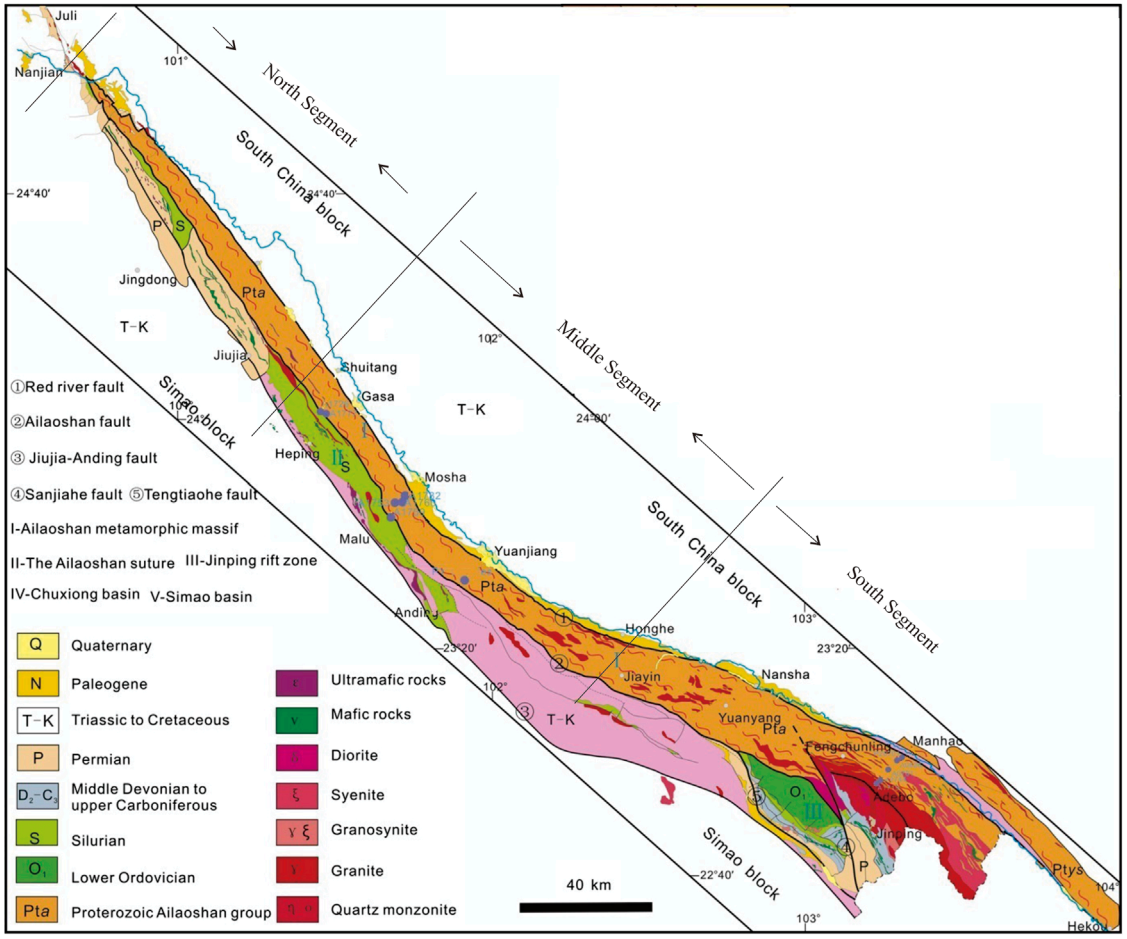

FIGURE 6
Geological map (modified from Liu et al., 2012).

Zone are all composed mainly of Proterozoic rocks (gneiss and amphibolite), with the strongest erosion resistance. Second, other rocks also have strong erosion resistance; for example, the main components of the Permian rocks are metamorphic sandstone and slate, the main components of the Silurian rocks are quartz sandstone, the main components of the Triassic rocks are slate, and the main components of the Ordovician rocks are slate and quartz sandstone. Third, combined with the DEM image in Figure 1, the highest elevation of the Ailaoshan Shear Zone in the study area is located in the Proterozoic strata. On the basis of the spatial distribution of various rocks and the location of the Yuanjiang Groove (Figure 2), it can be concluded that lithology was not the cause of the Yuanjiang Groove.

For climatic factors, in terms of precipitation, on the basis of data from the National Meteorological Data Center (https://data.cma.cn/data/weatherBk.html), we compiled the statistics of the 30-year annual precipitation in Dali, Yuanjiang and Honghe Counties for the period of 1981–2010. These three points represent the precipitation in the northern, middle and southern segments of the Ailaoshan Shear Zone, respectively. The statistics reveal that the average annual precipitation amounts in Dali, Yuanjiang and Honghe are 1054.8 mm, 806.6 mm and 832.5 mm, respectively. The precipitation amounts at the three locations did not significantly differ. In particular, the precipitation in Yuanyang and Honghe was basically the same. Therefore, rainfall is not the main cause of these geomorphic indices.

5.2 Effects of tectonic movements

The tectonic movements of the fault, including strike-slip movement and dip-slip movement, may also generate surface subsidence. There are two mechanisms by which strike-slip faults cause surface subsidence. First, in the area of terraces of strike-slip faults, pull-apart basins may have formed. Second, the area of bends in the strike-slip fault is prone to become an area of releasing bends that locally produces extension and surface subsidence. The surface subsidence formed under these two mechanisms was easier to identify. There is no large strike-slip fault on the west side of the Ailaoshan Shear Zone, so the surface subsidence in this study was not formed by the pull-apart effect. Similarly, we believe that the surface subsidence that formed in the releasing bend (SSRB) in this manuscript was not formed by the releasing bend effect for the following reasons. First, the SSRB was distributed mainly

along faults with relatively narrow widths (2–4 km in Wang et al., 2016). The surface subsidence in this manuscript (SSTM) extended at least to the top of the Ailaoshan Shear Zone (10–15 km). Second, the SSRB was distributed inside of the releasing bend, and the SSTM was distributed outside the releasing bend. Finally, surface subsidence caused by tension in the bend area of the slip fault should have occurred at the rear of the bend area (i.e., the northwestern area of Yuanjiang), which is inconsistent with the location of the releasing bend in this study. In summary, the pull-apart and releasing bend effects were not the causes of surface subsidence.

The dip-slip movement of a fault can cause uplift or subsidence of the hanging wall and footwall on either side of the fault. If the uplift or subsidence of different segments of the fault is not uniform, surface subsidence can also occur. In the ductile strike-slip movement of the Red River Fault, the Ailaoshan Shear Zone experienced large-scale uplift due to the presence of a dip-slip component (Harrison et al., 1992; 1996; Royden et al., 2008; Searle et al., 2010; Cao et al., 2011; Wang et al., 2020). The dip-slip movement of the Red River Fault has occurred mainly within the Eryuan–Midu segment of the fault. The dip-slip displacement in this segment is more than 1,500 m, with the dip-slip displacement near Dali exceeding 3,000 m. The dip-slip displacement of the Red River Fault within the Ailaoshan Shear Zone is much lower than that within the Eryuan–Midu segment. On the basis of the data from Guo et al. (2001), we plotted the uplift heights at different positions in the northern and middle segments of the Ailaoshan Shear Zone during the Quaternary, middle Pleistocene, and late Pleistocene (Figure 7). In every period, there are two characteristics of the uplift amount of the northern and middle segments of the Ailaoshan Shear Zone. First, from north to south, the uplift amount decreases in sequence, reflecting that the characteristic dip-slip rate of the Red River Fault gradually weakens from north to south. Second, the difference in uplift amounts at different locations is not significant, with the differences in the maximum uplift height during the Quaternary, middle Pleistocene, and late Pleistocene being approximately 100 m, 50 m, and 20 m, respectively. In terms of both trend and quantity, the formation of the Yuanjiang Groove was unlikely to be due to differential uplift of different segments of the Red River Fault.

5.3 Subsidence height

According to the results of a deep seismic wide-angle reflection section, the P-wave velocity of the crustal material on the east side of the Red River Fault is approximately 0.3 km/s greater than that on the west side of the Red River Fault (Bai and Wang, 2004; Zhang et al., 2013). According to the empirical relationship between the wave velocity and density, the density of crustal materials is approximately 0.1 ton/m^3 greater than the density on the west side (Christensen and Mooney, 1995). According to the Airy equilibrium model (Airy, 1855; Watts, 2001), relatively rigid and low-density crust floats on relatively plastic and dense mantle fluid (Figure 8A). When dense crust replaces less dense crust, the Earth's crust sinks (Figure 8B). After the replacement occurs, the height of the surface subsidence was calculated according to the following Equation 4:

$$\Delta h = \frac{\Delta \rho_c}{\rho_m} h \tag{4}$$

Here, $\Delta\rho_c$ was 0.1×10^3 kg/m^3, ρ_m was 3.3×10^3 kg/m^3, and when h was 20–30 km, Δh = 600~900 m. The tectonic subsidence height given by the ME$_n$ in this paper is approximately 600 m, and these two sets of data are in good agreement.

5.4 Height of the planation plane

Xiang et al. (2004) investigated the heights of planation planes on both sides of the Red River Fault. We extracted the planation surface data of the study area in this paper and plotted the data in Figure 9. This figure shows that the height of the planation plane in the northern segment of the Ailaoshan Shear Zone was between 2,700 and 3,000 m, and the height of the planation plane in the middle segment of the Ailaoshan Shear Zone was between 2,100 and 2,300 m. These data indicate that the height of the middle segment of the Ailaoshan Shear Zone decreased by 600–700 m. These data are close to the relatively flat surface obtained in this paper from the elevation-frequency data.

5.5 Comparison with geophysical exploration results

Zhang et al. (2013) deployed a deep seismic wide-angle reflection profile. The total length of the profile is approximately 360 km, and the seismic station spacing used to record seismic signals is approximately 3–5 km. Using these data, a 2D crustal velocity structure model along the cross section is obtained. The profile results reveal that the crust to the east of the Red River Fault crosses the Red River Fault and extrudes into the Ailaoshan Shear Zone by approximately 30–40 km. The accuracy of geophysical methods is strongly limited by the station spacing. In addition to the work of Zhang et al. (2013), the Himalaya-I Array is the densest seismic network deployed near the Yuanjiang Groove. The station spacing of this array is approximately 50 km near Yuanjiang (Li et al., 2016a). A little further away, Li and Gao (2023) deployed a seismic line in the northeast direction across the Red River Fault near Dadoumen, with a station spacing of approximately 20–30 km. The results for these stations may reflect the changes in trends in crustal parameters. For example, Li and Gao (2023) used the shear wave splitting method and proposed that crustal media differ on the west side of the Xiaojiang Fault zone and the northern segment of the Red River Fault zone. However, this approach may not be sufficient to detect the presence of the Yuanjiang Groove accurately.

Relying on the China Seismic Experimental Site (http://www.cses.ac.cn/) and the Major Earthquake Source Project of the China Earthquake Administration (www.eq-cedpc.cn/article/6975), we are carrying out two projects near the Yuanjiang Groove: the scientific deep drilling project (a borehole at a depth of 3,000 m across the Red River Fault) and the deep seismic wide-angle reflection profile (crossing the Red River Fault, with a total length of 100 km and a station spacing of 30 m). These projects are expected to be completed between 2025 and 2026. Researchers who are interested

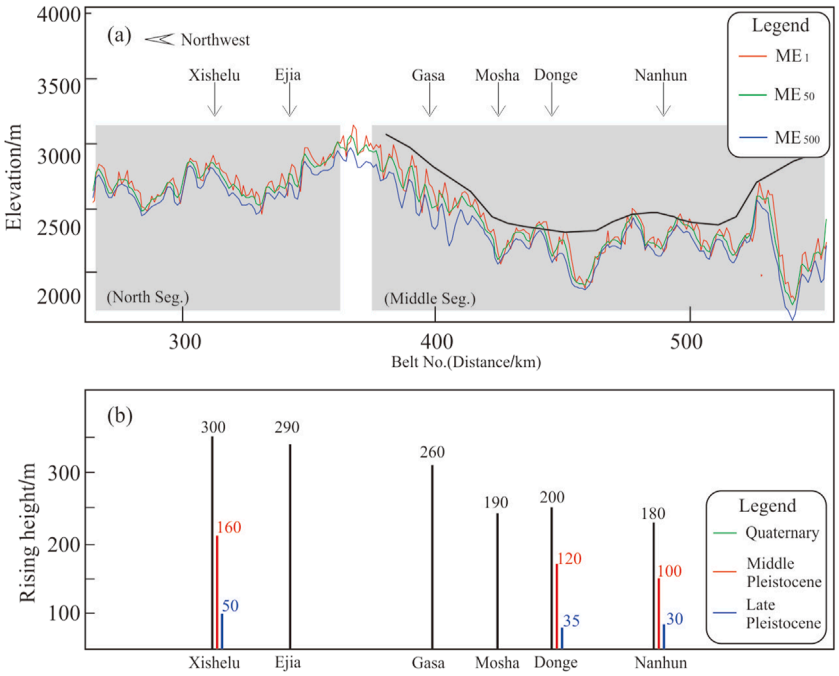

FIGURE 7
(A) Locations of geographic survey points within the Ailaoshan Shear Zone and **(B)** the uplift heights of the geographic survey points during the Quaternary (black), middle Pleistocene (red), and late Pleistocene (blue).

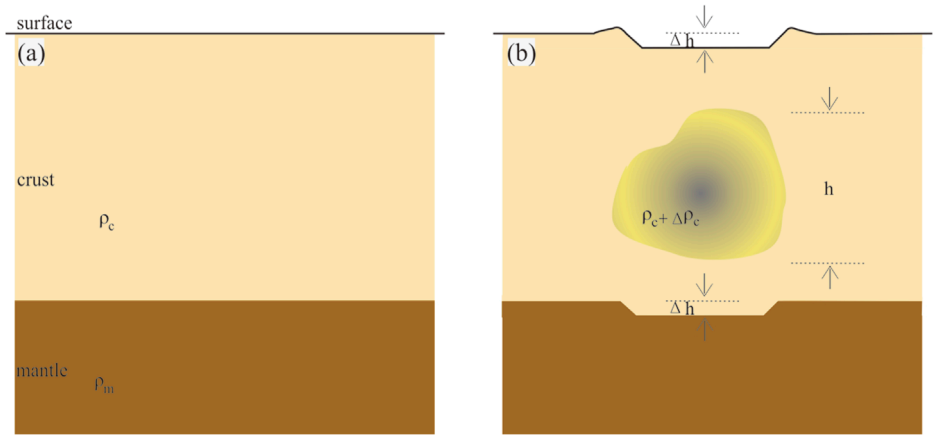

FIGURE 8
(A) Airy equilibrium model and **(B)** schematic diagram of crustal subsidence when dense crustal material replaces lower-density crustal material.

in the geodynamic model of this region can contact us to carry out joint research.

5.6 Start time of the extrusion event

The distance of the displacement of the Big Bend (Figure 1) on the Red River Fault was approximately 50 km (Wen et al., 2022), and the distance from which it extruded into the ASZ was approximately 30–40 km (Zhang et al., 2013). The left-lateral strike-slip rate of the southern Xiaojiang Fault is 6.8–7.2 mm/a (Han et al., 2017). Assuming that the average velocity of crustal movement is the same as the strike-slip rate of the southern segment of the Xiaojiang Fault, the start time of the Sichuan–Yunnan Block extruding into the Red River Fault was approximately 11–13 Ma. During the next 7 Ma, this extrusion caused the originally straight Red River Fault to bulge southwest, forming the Big Bend. The initial time at which the crust of the Sichuan–Yunnan Block crossed the Red River Fault and entered the Ailaoshan Shear Zone was approximately 4–6 Ma. Wang et al. (2016, 2020, 2022) used the low-temperature thermochronological method and existing thermochronological data to investigate the late Cenozoic exposition process and

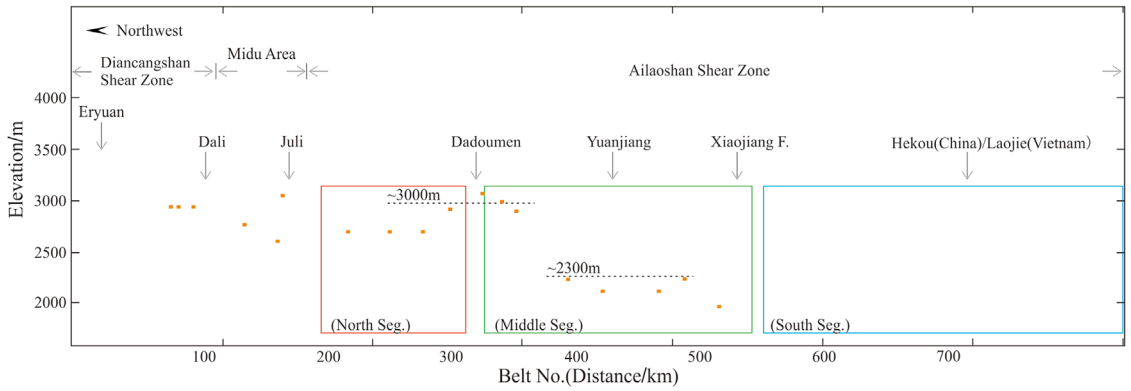

FIGURE 9
Height of the planation plane. The data were extracted from Xiang et al. (2004). The height of the planation plane in the northern segment of the Ailaoshan Shear Zone was approximately 2,700–3,000 m, and the height of the planation plane in the middle segment of the Ailaoshan Shear Zone was approximately 2,100–2,300 m.

exposition mechanisms of the Ailaoshan Shear Zone. Their study suggested that the tectonic inversion time of each segment of the Red River Fault was inconsistent; the tectonic inversion time of the southern segment was earlier than that of the northern segment, whereas the tectonic inversion time of the middle segment (near Yuanjiang) was approximately 14–10 Ma. The start time of sinistral movement in the Sichuan–Yunnan Block in this study is very close to these data. Therefore, we believe that the tectonic inversion time of the Red River Fault was approximately 11–13 Ma.

5.7 Geodynamic model

During the strike-slip movement of the Red River Fault, there was also normal movement. The long-term lithospheric extension and subsequent isostatic adjustment in this area produced a metamorphic core complex (MCC), which is the Ailaoshan Shear Zone. Low-temperature thermochronological data indicate that the Ailaoshan Shear Zone experienced rapid uplift during two periods: 22–17 Ma and 14–10 Ma. During these periods, rocks in the Ailaoshan Shear Zone experienced at least 400°C and 100°C of cooling, respectively (Leloup et al., 2001; Cao et al., 2011; Wang et al., 2020; 2022). A temperature of 500° means that the Ailaoshan Shear Zone has risen by at least 30–40 km (An and Shi, 2007); that is, the materials in the Ailaoshan Shear Zone may come from the lower crust or even the mantle. During the process of MCC doming, the upwelling of hot and soft material resulted in softer material on the west side of the Red River Fault than on the east side at middle and lower crustal depths. When the force of extrusion broke through the barrier of the Red River Fault, the harder and denser material from the middle and lower crust on the east side of the Red River Fault entered the base of the Ailaoshan Shear Zone, resulting in surface subsidence. On the basis of the geomorphological research results and the geophysical research results in this paper, we can preliminarily establish a geodynamic model of the area of intersection of the Red River Fault and the Xiaojiang Fault on the southeastern margin of the Tibetan Plateau since the middle Miocene.

The first stage occurred before ~13–10 Ma. During this stage, the tectonic evolutionary model of the southeastern margin of the Tibetan Plateau involved mainly radial extrusion, the faults on the west side of the Red River Fault were mainly dip-slip, and some faults had a small strike-slip component. During this stage, the movement of the Red River Fault involved left-lateral strike-slip motion combined with normal slip motion (Figure 10A). The long-term and large-scale lithospheric extension led to the dominance of mantle and middle–lower crustal materials under the Ailao Mountains, forming the MCC. The magnitude of the doming may have reached 30–40 km (Figure 10B).

In the second stage, from the period of tectonic inversion to 6–4 Ma, the materials from the Tibetan Plateau flowed clockwise into the Sichuan–Yunnan Block around the East Himalayan Syntax. The extrusion caused the Red River Fault to bend, resulting in the big bend. The extrusion lasted for approximately 7 Ma, and the extrusion speed was approximately 7 mm/a. This process caused the Red River Fault (Ailaoshan Shear Zone) to bulge southwest, with a ductile bending distance of up to 50 km (Figure 10C). Owing to the different hardnesses of the crustal layers below the Ailaoshan Shear Zone, the resistance experienced by the crustal layers to the east of the Red River Fault also varies. This stage still experienced stress and strain accumulation, and the layers of the eastern crust have not yet been decoupled (Figure 10D).

During the third stage, from 6 to 4 Ma, due to the accumulation of stress, the strength of extrusion in the crust further increased. The middle crust and upper crust were decoupled; the upper crust was still blocked by the Ailaoshan Shear Zone, while the middle and lower crust extruded into the Ailaoshan Shear Zone. Because the density of the material squeezed into the Ailaoshan Shear Zone was slightly greater than that of the original material, surface subsidence of hundreds of meters occurred in the Ailaoshan Shear Zone during this stage (Figure 10F). The extrusion speed at this stage was roughly the same as that at the previous stage, at approximately 7 mm/a, and the extrusion distance was approximately 30–40 km (Figure 10E). The horizontal position of the front of extrusion was approximately 40 km from the northwest of the Yuanjiang River to approximately 60 km southeast of the Yuanjiang River.

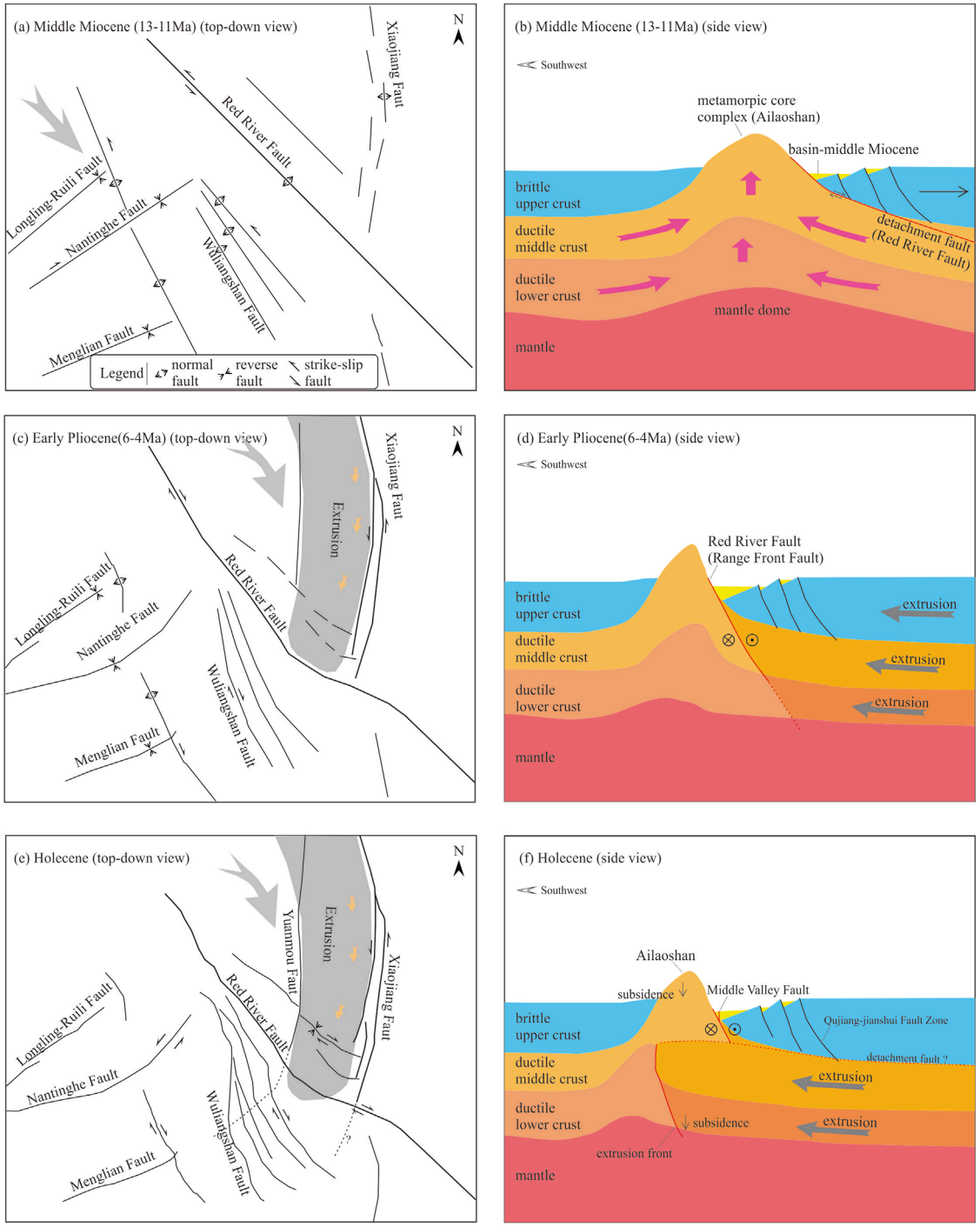

FIGURE 10
Geodynamic model of the area of intersection of the Xiaojiang Fault and the Red River Fault. Top-down view and side view of the first stage **(A,B)**, second stage **(C,D)**, and third stage **(E,F)**. The black lines represent the faults, the thick black lines represent the main boundary faults, the large gray arrows represent the direction of the main compressive stress, the gray areas represent the range of extrusion, the small yellow arrows represent the direction of extrusion, and the dotted lines represent the speculated hidden faults.

According to the Global Navigation Satellite System (GNSS) observation results, the slip rates on the two sides of the Xiaojiang Fault are quite different; therefore, the eastern boundary of the extrusion should be the Xiaojiang Fault. The width of the Yuanjiang Groove (100 km), west of the Xiaojiang Fault, is approximately 100 km, which is approximately the Yuanmou Fault. The shear rate and rotation rate calculated by the GNSS, as well as the shear wave splitting, Q value, P wave velocity, and S wave velocity, reveal significant differences in the geophysical properties of the crust on both sides of the Yuanmou Fault. Accordingly, it is speculated that the Yuanmou Fault is the western boundary of the extrusion, but this conclusion still needs more data for support.

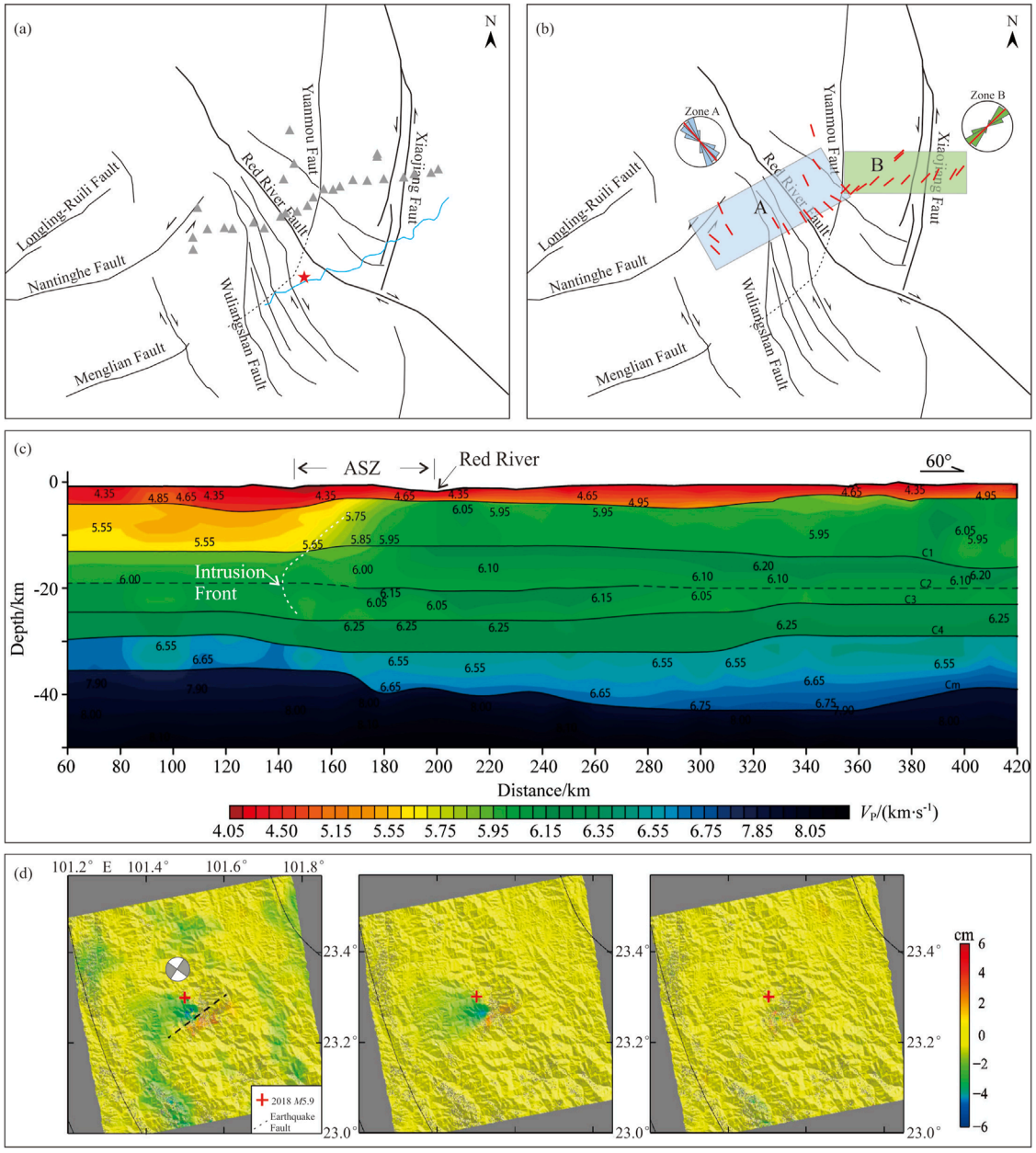

FIGURE 11
Research results of other disciplines. **(A)** The gray triangles indicate the locations of seismic stations in Li and Gao (2023); the blue line indicates the deep seismic wide-angle reflection/refraction profile in Zhang et al. (2013); the red five-pointed star indicates the location of the 2018 Ms5.9 earthquake. **(B)** Direction of fast waves resulting from crustal shear wave splitting, modified from Li and Gao (2023). **(C)** High-precision P-wave velocity structure of the crust, modified from Zhang et al. (2013). **(D)** InSAR coseismic deformation, modified from Sun and Liu (2019); the result of the focal mechanism solution is cited from Li et al. (2020).

The geodynamic models given here are very preliminary and rough, and there is still much work to be completed in the future. We will also carry out some work in this area to improve and refine this model.

5.8 Research results of other disciplines

Zhang et al. (2013) deployed a deep seismic wide-angle reflection/refraction profile between Puer and Luxi (see the blue line in Figure 11A for the location of the survey line). On this survey line, the spacing between the blasting signal receiving stations is approximately 4 km; therefore, the high-precision P-wave velocity structure of the crust under the survey line is obtained (Figure 11C). The velocity structure diagram shows that the crust on the northeast side of the Red River Fault extruded into the ASZ southwest of the fault. This research result is thus far the first evidence that directly supports the model in this paper.

On the basis of the data of a seismic station that crosses the Red River Fault and the Xiaojiang Fault (the locations of seismic

stations are shown as gray triangles in Figure 11A), Li and Gao (2023) obtained the direction of fast waves of crustal shear wave splitting data under the survey line (Figure 11B). On the basis of the distribution of fast crustal shear waves, the directions of fast waves on the west side and east side of the Yuanmou Fault are nearly orthogonal. This finding indicates that the crust on the two sides of the Yuanmou Fault is significantly different; that is, this fault may be an important boundary fault. This result is consistent with the model proposed in this paper.

On 8 September 2018, an earthquake with a magnitude of 5.9 occurred approximately 60 km southwest of Yuanjiang County (see the red five-pointed star in Figure 10A for the earthquake location). After the earthquake, similar focal mechanism solutions were given by multiple institutions. The two nodal planes of the focal mechanism solution run NE and northwest (see the left diagram of Figure 11D for the focal mechanism solution). According to the local fault distribution, intuitively, the seismogenic fault of this earthquake should have been the northwest-trending Wuliangshan Fault. However, according to seismic waveform analysis (Li et al., 2020) and InSAR coseismic deformation studies (Sun and Liu, 2019), the seismogenic fault of this earthquake should be a concealed fault in the northeastern direction—which is consistent with the model proposed in this paper.

In the past 10 years, many seismic tomography results have been produced near the study area, and these results have deepened our understanding of the crustal structure of the study area and nearby areas (e.g., Liu et al., 2023; Wang et al., 2024). However, the lack of seismic tomography data strongly supports the existence of a middle–lower crustal low-velocity layer between the Yuanmou Fault and the Xiaojiang Fault. We speculate that there may be two reasons for this. First, the seismic station spacing used for seismic tomography is too large. Second, the velocity difference between the material inside the crust and the material on both sides of the crust is too small (only 0.3 km/s). The specific reason needs further study.

According to the model in this paper, there should be a thrust-type focal mechanism solution at the extrusion front, but we have not yet observed it. We also did not observe a solution for the strike-slip focal mechanism at the extrusion front. This may be because the seismic station spacing in this area is relatively large, small-magnitude earthquakes could not be observed, and the focal mechanism solutions could not be retrieved.

In summary, although some research results support our model, in general, more observations and a denser seismic network are needed to obtain a more accurate estimate of the crustal structure of the study area, thus proving or disproving the proposed geodynamic model in this paper.

6 Conclusion

On the basis of the above analysis and discussion, the following conclusions can be drawn:

(1) The geomorphic parameters of the middle segment of the Ailaoshan Shear Zone near Yuanjiang were quite different from those of the northern and southern segments. After removing the influences of rock properties, climate and other factors, we believe that the main cause is surface subsidence caused by crustal extrusion.

(2) On the basis of existing data and the Airy isostatic crustal model, the calculated theoretical settlement height is approximately 600–900 m, which is close to the ME_n and the height of the planation plane.

(3) A geodynamic model near the southeastern margin of the Tibetan Plateau was constructed. In the mid-Miocene, tectonic inversion of the Red River Fault occurred. After tectonic inversion, material from the Tibetan Plateau moved into the Sichuan–Yunnan Block around the Eastern Himalayan Syntax, and the resulting extrusion caused the Red River Fault to bend ductility by 50 km. The crust extruded through the barrier and entered the interior of the Ailaoshan Shear Zone; the current distance of extrusion into the Ailaoshan Shear Zone is approximately 30–40 km.

(4) Because of the middle and lower crust extrusions, the role of the Red River Fault as the boundary has weakened. That also implies that the Big Bend section of the Red River Fault and the Qujiang-Jianshui Fault Zone to its north have a similar seismic tectonic environment and seismic risks.

Data availability statement

The original contributions presented in the study are included in the article/supplementary material, further inquiries can be directed to the corresponding author.

Author contributions

QZ: Conceptualization, Data curation, Formal Analysis, Funding acquisition, Investigation, Methodology, Project administration, Resources, Software, Supervision, Validation, Visualization, Writing–original draft, Writing–review and editing.

Funding

The author(s) declare that financial support was received for the research, authorship, and/or publication of this article. This work was supported by the Earthquake Science and Technology Innovation Team of the Yunnan Earthquake Agency (CXTD202408) and the Key Research and Development Plan of Yunnan Province (No. 202203AC100003).

Acknowledgments

I would like to thank Suge He, Jingnan Liu, Peng Tian, Changwei Liu, and Weidong Luo for their valuable suggestions during the paper revision process.

Conflict of interest

The author declares that the research was conducted in the absence of any commercial or financial relationships that could be construed as a potential conflict of interest.

Publisher's note

All claims expressed in this article are solely those of the authors and do not necessarily represent those of their affiliated organizations, or those of the publisher, the editors and the reviewers. Any product that may be evaluated in this article, or claim that may be made by its manufacturer, is not guaranteed or endorsed by the publisher.

References

Airy, G. B. (1855). On the computation of the effect of the attraction of mountain-masses, as disturbing the apparent astronomical latitude of stations in geodetic surveys. *Philosophical Trans. R. Soc. Lond.* 145, 101–104. doi:10.1098/rstl.1855.0003

An, M., and Shi, Y. (2007). Three-dimensional thermal structure of the Chinese continental crust and upper mantle. *Sci. China Ser. D Earth Sci.* 50, 1441–1451. doi:10.1007/s11430-007-0071-3

Bai, Z., and Wang, C. (2004). Tomography research of the Zhejiang-Binchuan and Menglian-Malong wide-angle seismic profiles in Yunnan province. *Chin. J. Geophys.* 2, 257–267. doi:10.3321/j.issn:0001-5733.2004.02.012

Burchfiel, B. C., and Chen, Z. (2012) *Tectonics of the southeastern Tibetan Plateau and its adjacent foreland*, 210. Boulder, Colorado: Geological Society of America Publications, 1–231. Available at: https://pubs.geoscienceworld.org/gsa/books/book/212/Tectonics-of-the-Southeastern-Tibetan-Plateau-anddoi:10.1130/MEM210

Burrough, P. A., and Mcdonnell, R. (1998). *Principles of geographical information systems*. Oxford University Press.

Cao, S. Y., Neubauer, F., Liu, J. L., Genser, J., and Leiss, B. (2011). Exhumation of the diancang Shan metamorphic complex along the Ailao Shan-Red River belt, southwestern yunnan, China: evidence from $^{40}Ar/^{39}Ar$ thermochronology. *J. Asian Earth Sci.* 42, 525–550. doi:10.1016/j.jseaes.2011.04.017

Chen, Z., Burchfiel, B., Liu, Y., King, R. W., Royden, L. H., Tang, W., et al. (2000). Global Positioning System measurements from eastern Tibet and their implications for India/Eurasia intercontinental deformation. *J. Geophys. Res. Solid Earth* 105, 16215–16227. doi:10.1029/2000jb900092

Christensen, N. I., and Mooney, W. D. (1995). Seismic velocity structure and composition of the continental crust: a global view. *J. Geophys. Res.* B7, 9761–9788. doi:10.1029/95JB00259

Copley, A. (2008). Kinematics and dynamics of the southeastern margin of the Tibetan Plateau. *Geophys. J. Int.* 174, 1081–1100. doi:10.1111/j.1365-246x.2008.03853.x

Deng, J., Wang, Q., Li, G., and Santosh, M. (2014). Cenozoic tectono-magmatic and metallogenic processes in the Sanjiang region, southwestern China. *Earth Sci. Rev.* 138, 268–299. doi:10.1016/j.earscirev.2014.05.015

Dong, S., Han, Z., Guo, P., Xie, Z., and Yin, X. (2023). Seismological research in yunnan province, China, and its tectonic implication between the Xianshuihe-Xiaojiang fault system and the Red RiverRiver Fault zone. *Front. Earth Sci.* 11, 1239689. doi:10.3389/feart.2023.1239689

Finlayson, A. (2013). Digital surface models are not always representative of former glacier beds: palaeoglaciological and geomorphological implications. *Geomorphology* 194, 25–33. doi:10.1016/j.geomorph.2013.03.026

Flesch, L. M., Haines, A. J., and Holt, W. E. (2001). Dynamics of the India-Eurasia collision zone. *J. Geophys. Res. Solid Earth* 106, 16435–16460. doi:10.1029/2001jb000208

Gan, W., Molnar, P., Zhang, P., Xiao, G., Liang, S., Zhang, K., et al. (2022). Initiation of clockwise rotation and Eastward Transport of southeastern Tibet inferred from deflected fault traces and GPS observations. *Geol. Soc. Am.* 134, 1129–1142. doi:10.1130/B36069.1

Guo, P., Han, Z., Dong, S., Mao, Z., Hu, N., Gao, F., et al. (2021). Latest quaternary active faulting and paleoearthquakes on the southern segment of the Xiaojiang Fault Zone, SE Tibetan plateau. *Lithosphere* 2021, 7866379. doi:10.2113/2021/7866379

Guo, S., Xiang, H., Ji, F., and Zhang, W. (1996). A study on the relation between Quaternary right-lateral slip and tip extension along the Red River Fault. *Seismol. Geol.* 18, 301–309. Available at: https://www.dzdz.ac.cn/CN/Y1996/V18/I4/301.

Guo, S. M., Ji, F. J., Xiang, H. F., Dong, X. Q., Yan, F. H., Zhang, S. L., et al. (2001). *Red River avtive Fault Zone*. 7-5027-5300-1. Beijing: China Ocean Press.

Hamdouni, R. E., Irigaray, C., Fernández, T., Chacon, J., and Keller, E. A. (2008). Assessment of relative active tectonics, southwest border of the Sierra Nevada (southern Spain). *Geomorphology* 96, 150–173. doi:10.1016/j.geomorph.2007.08.004

Han, Z., Dong, S., Mao, Z., Hu, N., Tan, X., Yuan, R., et al. (2017). The Holocene activity and strike-slip rate of the southern segment of Xiaojiang Fault in the southeastern Yunnan region, China. *Seismol. Geol.* 39, 1–19. doi:10.3969/j.issn.0253-4967.2017.01.001

Harrison, T. M., Leloup, P. H., Ryerson, F. J., Tapponnier, P., Lacassin, R., and Wenji, C. (1996). "Diachronous initiation of transtension along Ailao Shan-Red River Shear zone, Yunnan and Vietnam," in *Tectonic evolution of Asia*. Editors Y. An, and T. Harrison (New York: Cambridge University Press), 208–226.

Harrison, T. M., Wenji, C., Leloup, P. H., Ryerson, F. J., and Tapponnier, P. H. (1992). An early Miocene transition in deformation regime within the Red River Fault zone, Yunnan, and its significance for Indo-Asian tectonics. *J. Geophys. Res.* 97, 7159–7182. doi:10.1029/92JB00109

He, H., Li, P., and Fang, Z. (1992). Analysis of seismogenic conditions in the wedge tectonic region of southeast Yunnan Province. *Seismol. Geol.* 14, 217–226. Available at: https://www.dzdz.ac.cn/CN/Y1992/V14/I3/217.

Horton, R. E. (1945). Erosional development of streams and their drainage basins, hydrophysical approach to quantitative morphology. *Bull. Geol. Soc. Am.* 56, 275–370. doi:10.1130/0016-7606(1945)56[275:edosat]2.0.co;2

Hu, M., Wu, Z., Li, J., and Huang, X. (2023). The late Quaternary strike-slip rate of the Qiaojia segment of the Xiaojiang Fault zone. *Acta Geol. Sin.* 97, 16–29. doi:10.19762/j.cnki.dizhixuebao.2022188

Jotheri, J., de Gruchy, M. W., Almaliki, R., and Feadha, M. (2019). Remote sensing the archaeological traces of boat movement in the marshes of southern mesopotamia. *Remote Sens.* 11, 2474. doi:10.3390/rs11212474

Jotheri, J., Feadha, M., Al-Janabi, J., and Alabdan, R. (2022). Landscape archaeology of southern mesopotamia: identifying features in the dried marshes. *Sustainability* 14, 10961. doi:10.3390/su141710961

Kirby, E., Whipple, K. X., Tang, W., and Chen, Z. (2003). Distribution of active rock uplift along the eastern margin of the Tibetan Plateau: inferences from bedrock channel longitudinal profiles. *J. Geophys. Res.* 108, 2217. doi:10.1029/2001JB000861

Lacassin, R., Replumaz, A., and Leloup, P. H. (1998). Hairpin river loops and slipsense inversion on southeast Asian strike-slip faults. *Geology* 26, 703–706. doi:10.1130/0091-7613(1998)026<0703:hrlass>2.3.co;2

Leloup, P. H., Arnaud, N., Lacassin, R., Kienast, J. R., Harrison, T. M., Trong, T. T. P., et al. (2001). New constraints on the structure, thermochronology, and timing of the Ailao Shan-Red River shear zone, SE Asia. *J. Geophys. Res.* 106, 6683–6732. doi:10.1029/2000JB900322

Leloup, P. H., Lacassin, R., Tapponnier, P., Scharer, U., Zhong, D., Liu, X., et al. (1995). The Ailao Shan-Red River shear zone (Yunnan, China), tertiary transform boundary of Indo-China. *Tectonophysics* 251, 3–84. doi:10.1016/0040-1951(95)00070-4

Leloup, P. H., Tapponnier, P., Lacassin, R., and Searle, M. (2007). Discussion on the role of the Red River Shear zone, yunnan and Vietnam, in the continental extrusion of SE asia *Journal*, Vol. 163, 2006, 1025–1036. *J. Geol. Soc.* 164, 1253–1260. doi:10.1144/0016-76492007-065

Li, L., Wang, B., Peng, Z., and Wang, W. (2016a). Seismic detections of the 15 February 2013 Chelyabinsk meteor from the dense ChinArray. *Earth Sci.* 29 (4), 221–233. doi:10.1007/s11589-016-0159-y

Li, P., and Wang, L. (1975). Exploration of the seismo-geological features of the Yunnan-west Sichuan region. *Chin. J. Geol.* 10, 308–326. Available at: http://www.dzkx.org/CN/abstract/abstract8698.shtml.

Li, X., Ran, Y. K., Chen, L. C., Wang, H., Yu, J., Zhang, Y. Q., et al. (2016b). The Holocene seismic evidence on the southern segment of the Red River Fault zone. *Seismol. Geol.* 38, 596–604. doi:10.3969/j.issn.0253-4967.2016.03.007

Li, Y., and Gao, Y. (2023). Rigid widths of active block boundary faults and crustal layered anisotropy in the intersection of faults Honghe and Xiaojiang in the SE margin of the Tibetan Plateau. *Geophys. J. Int.* 235, 1504–1518. doi:10.1093/gji/ggad279

Li, Z. X., Wan, Y. G., Cui, H. W., Li, Z. Y., Hu, X. H., Huang, J. C., et al. (2020). Characteristics analysis of tectonic stress field around the Mojiang earthquake and its adjacent areas on September 8, 2018. *Chin. J. Geophys.* 63, 1431–1443. doi:10.6038/cjg2020N0155

Lidmar-Bergström, K. (1996). Long term morphotectonic evolution in Sweden. *Geomorphology* 16, 33–59. doi:10.1016/0169-555X(95)00083-H

Liu, J., Ding, L., Zeng, L., Tapponnier, P., and Gaudemer, Y. (2006). Large-scale terrain analysis of selected regions of the Tibetan plateau:discussion on the origin of plateau planation surface. *Earth Sci. Front.* 13, 285–299. doi:10.3321/j.issn:1005-2321.2006.05.002

Liu, J. L., Tang, Y., Tran, M. D., Cao, S., Zhao, L., Zhang, Z. C., et al. (2012). The nature of the Ailao Shan-Red River (ASRR) shear zone: constraints from structural, microstructural and fabric analyses of metamorphic rocks from the Diancang

Shan, Ailao Shan and Day Nui Con Voi massifs. *J. Asian Earth Sci.* 47, 231–251. doi:10.1016/j.jseaes.2011.10.020

Liu, Y., Yu, Z., Zhang, Z., Yao, H., Wang, W., Zhang, H., et al. (2023). The high-resolution community velocity model V2.0 of southwest China, constructed by joint body and surface wave tomography of data recorded at temporary dense arrays. *Sci. China Earth Sci.* 66, 2368–2385. doi:10.1007/s11430-022-1161-7

Liu-Zeng, J., Tapponnier, P., Gaudemer, Y., and Ding, L. (2008). Quantifying landscape differences across the Tibetan Plateau: implications for topographic relief evolution. *J. Geophys. Res.* 113, F04018. doi:10.1029/2007JF000897

Macmillan, R. A., Pettapiece, W. W., Nolan, S. C., and Goddard, T. W. (2000). A generic procedure for automatically segmenting landforms into landform elements using DEMs, heuristic rules and fuzzy logic. *Fuzzy Sets Syst.* 113, 81–109. doi:10.1016/S0165-0114(99)00014-7

Millán, H., Bezemer, T. D., Verges, J., Marzo, M., Munoz, J. A., Roca, E., et al. (1995). Palaeo-elevation and effective elastic thickness evolution at mountain ranges: inferences from flexural modelling in the Eastern Pyrenees and Ebro Basin. *Mar. and Petroleum Geol.* 12, 917–928. doi:10.1016/0264-8172(95)98855-Y

Molnar, P., and Tapponnier, P. (1975). Cenozoic Tectonics of Asia: effects of a Continental Collision: features of recent continental tectonics in Asia can be interpreted as results of the India-Eurasia collision. *Science* 189, 419–426. doi:10.1126/science.189.4201.419

Peltzer, G., and Tapponnier, P. (1988). Formation and evolution of strike-slip faults, rifts, and basins during the India-asia collision: an experimental approach. *J. Geophys. Res. Solid Earth* 93, 15085–15117. doi:10.1029/jb093ib12p15085

Qian, Y., Xiong, L., Li, J., and Tang, G. (2016). Landform planation index extracted from DEMs: a Case study in Ordos platform of China. *Chin. Geogr. Sci.* 26, 314–324. doi:10.1007/s11769-016-0811-4

Qiu, L., Yan, D. P., Tang, S. L., Wang, Q., Yang, W. X., Tang, X., et al. (2016). Mesozoic geology of Southwestern China: indosinian foreland overthrusting and subsequent deformation. *J. Asian Earth Sci.* 122, 91–105. doi:10.1016/j.jseaes.2016.03.006

Ren, Z. (2013). Geometry and deformation features of the most recent co-seismic surface ruptures along the Xiaojiang Fault and its tectonic implications for the Tibetan Plateau. *J. Asian Earth Sci.* 77, 21–30. doi:10.1016/j.jseaes.2013.08.016

Replumaz, A., Lacassin, R., Tapponnier, P., and Leloup, P. (2001). Large river offsets and plio-quaternary dextral slip rate on the Red River Fault (yunnan, China). *J. Geophys. Res.* 106, 819–836. doi:10.1029/2000jb900135

Replumaz, A., and Tapponnier, P. (2003). Reconstruction of the deformed collision zone between India and Asia by backward motion of lithospheric blocks. *J. Geophys. Res. Solid Earth* 108, 1978–2012. doi:10.1029/2001jb000661

Roger, F., Calassou, S., Lancelot, J., Malavieille, J., Mattauer, M., Xu, Z., et al. (1995). Miocene emplacement and deformation of the konga Shan granite (Xianshui He fault zone, west Sichuan, China): geodynamic implications. *Earth Planet. Sci. Lett.* 130, 201–216. doi:10.1016/0012-821x(94)00252-t

Royden, L. H., Burchfiel, B. C., King, R. W., Wang, E., Chen, Z., Shen, F., et al. (1997). Surface deformation and lower crustal flow in eastern Tibet. *Science* 276, 788–790. doi:10.1126/science.276.5313.788

Royden, L. H., Burchfiel, B. C., and van der Hilst, R. D. (2008). The geological evolution of the Tibetan plateau. *Science* 321, 1054–1058. doi:10.1126/science.1155371

Schmidt, K. M., and Montgomery, D. R. (1995). Limits to relief. *Science* 270, 617–620. doi:10.1126/science.270.5236.617

Schoenbohm, L. M., Burchfiel, B. C., and Liangzhong, C. (2006). Propagation of surface uplift, lower crustal flow, and Cenozoic tectonics of the southeast margin of the Tibetan Plateau. *Geology* 34, 813–816. doi:10.1130/g22679.1

Schoenbohm, L. M., Whipple, K. X., Burchfiel, B. C., and Chen, L. (2004). Geomorphic constraints on surface uplift, exhumation, and plateau growth in the Red River region, Yunnan Province, China. *Geol. Soc. Am. Bull.* 116, 895–909. doi:10.1130/b25364.1

Searle, M. P., Yeh, M. W., Lin, T. H., and Chung, S. L. (2010). Structural constraints on the timing of left-lateral shear along the Red River Shear zone in the Ailao Shan and diancang Shan ranges, Yunnan, SW China. *Geosphere* 6, 316–338. doi:10.1130/GES00580.1

Shen, Z. K., Lü, J., Wang, M., and Bürgmann, R. (2005). Contemporary crustal deformation around the southeast borderland of the Tibetan Plateau. *J. Geophys. Res. Solid Earth* 110, 1978–2012. doi:10.1029/2004jb003421

Shi, X., Wang, Y., Sieh, K., Weldon, R., Feng, L., Chan, C. H., et al. (2018). Fault slip and GPS velocities across the Shan plateau define a curved Southwestward crustal motion around the eastern Himalayan Syntaxis. *J. Geophys. Res. Solid Earth* 123, 2502–2518. doi:10.1002/2017jb015206

Simons, W. J. F., Socquet, A., Vigny, C., Ambrosius, B. A. C., Haji Abu, S. H., Promthong, C., et al. (2007). A decade of GPS in southeast asia: resolving sundaland motion and boundaries. *J. Geophys. Res. Solid Earth* 112, B06420. doi:10.1029/2005jb003868

Song, F., and Wang, Y. (1998). *The active Xiaojiang Fault zone*. Beijing: Seismological Press.

Strahler, A. N. (1950). Equilibrium theory of erosional slopes approached by frequency distribution analysis; Part 1. *Am. J. Sci.* 248, 673–696. doi:10.2475/ajs.248.10.673

Sun, H., and Liu, C. (2019). InSAR coseismic deformation mechanism of Yunnan Mojiang Ms 5.9 earthquake in 2018. *J. Seismol. Res.* 42, 379–384. doi:10.3969/j.issn.1000-0666.2019.03.010

Tapponnier, P., Lacassin, R., Leloup, P. H., Scharer, U., Zhong, D., Wu, H., et al. (1990). The Ailao Shan/Red River metamorphic belt: tertiary left-lateral shear between Indochina and south China. *Nature* 343, 431–437. doi:10.1038/343431a0

Tapponnier, P., Peltzer, G., Dain, A. Y. L., Armijo, R., and Cobbold, P. (1982). Propagating extrusion tectonics in Asia:New insights from simple experiments with plasticine. *Geology* 10, 611–616. doi:10.1130/0091-7613(1982)10<611:petian>2.0.co,2

Wang, E., Burchfiel, B. C., Royden, L. H., Chen, L., Chen, J., Li, W., et al. (1998) "Late Cenozoic Xianshuihe-Xiaojiang, Red River, and Dali fault systems of southwestern Sichuan and central Yunnan, China,". Boulder, Colorado: Geological Society of America. doi:10.1130/0-8137-2327-2.1

Wang, M., and Shen, Z. (2020). Present day crustal deformation of continental China Derived from GPS and its tectonic implications. *J. Geophys. Res. Solid Earth* 125 (2). doi:10.1029/2019JB018774

Wang, X., Chen, L., and Chen, Q. F. (2024). Evaluation of 3D crustal seismic velocity models in southwest China: model performance, limitation, and prospects. *Sci. China Earth Sci.* 67, 604–619. doi:10.1007/s11430-023-1215-1

Wang, Y., Wang, Y., Schoenbohm, L. M., Zhang, P., Zhang, B., Sobel, E. R., et al. (2020). Cenozoic exhumation of the Ailaoshan-Red River shear zone: new insights from low-temperature thermochronology. *Tectonics* 39, e06151. doi:10.1029/2020TC006151

Wang, Y., Wang, Y., Zhang, P., Zhang, J., Zhang, B., Liu-Zeng, J., et al. (2022). Cenozoic tectonic evolution of regional fault systems in the SE Tibetan Plateau. *Sci. China Earth Sci.* 65, 601–623. doi:10.1007/s11430-021-9880-3

Wang, Y., Zhang, B., Schoenbohm, L. M., Zhang, J., Zhou, R., Hou, J., et al. (2016). Late cenozoic tectonic evolution of the Ailao Shan-Red River Fault (SE Tibet): implications for kinematic change during plateau growth. *Tectonics* 35, 1969–1988. doi:10.1002/2016TC004229

Watts, A. B. (2001). *Isostasy and flexure of the lithosphere*. Cambridge: Cambridge University Press.

Wen, X., Du, F., Long, F., Fan, J., and Zhu, H. (2011). Tectonic dynamics and correlation of major earthquake sequences of the Xiaojiang and Qujiang-Shiping fault systems, Yunnan, China. *Sci. China Ser. D. Earth Sci.* 41, 1563–1575. doi:10.1007/s11430-011-4231-0

Wen, X., Ma, S., Fang, L., Liang, M., Du, F., Long, F., et al. (2022). Complex structural fault system and distributed deformation across the big bend of the Red River Fault, Yunnan, China. *Phys. Earth Planet. Interiors* 333, 106942. doi:10.1016/j.pepi.2022.106942

Whipple, K. X., Kirby, E., and Brocklehurst, S. H. (1999). Geomorphic limits to climate-induced increases in topographic relief. *Nature* 401, 39–43. doi:10.1038/43375

Whipple, K. X., and Tucker, G. E. (1999). Dynamics of the stream-power river incision model: implications for height limits of mountain ranges, landscape response timescales, and research needs. *J. Geophys. Res. Solid Earth* 104, 17661–17674. doi:10.1029/1999JB900120

Widdowson, M. (1997) The geomorphological and geological importance of palaeosurfaces, London, Special Publications: Geological Society, 120. 1–12. doi:10.1144/GSL.SP.1997.120.01.01

Wu, Z., Long, C., Fan, T., Zhou, C., Feng, H., Yang, Z., et al. (2015). The arc rotationalshear active tectonic system on the southeastern margin of Tibetan Plateau and its dynamic characteristics and mechanism. *Geol. Bull. China* 34, 1–31. doi:10.3969/j.issn.1671-2552.2015.01.002

Xiang, H., Han, Z., Guo, S., Zhang, W., and Chen, L. (2004). Large-scale dextral strike-slip movement and associated tectonic deformation along the Red-River Fault Zone. *Seismol. Geol.* 26, 597–610. doi:10.3969/j.issn.0253-4967.2004.04.006

Xu, X., Wen, X., Zheng, R., Ma, W., Song, F., and Yu, G. (2003). Pattern of latest tectonic motion and its dynamics for active blocks in Sichuan- Yunnan region, China. *Sci. China (Series D)* 33, 210–226. doi:10.1360/03dz0017

Xu, Z., Li, H., Tang, Z., Qi, X., Li, H., and Cai, Z. (2011a). The transformation of the terrain structures of the Tibetan Plateau through large-scale strike-slip faults. *Acta Petrol. Sin.* 27, 3157–3170. Available at: http://www.ysxb.ac.cn/article/id/aps_20111101.

Xu, Z., Yang, J., Li, H., Ji, S., Zhang, Z., and Liu, Y. (2011b). On the tectonics of the India-asia collision. *Acta Geol. Sin.* 85, 1–33. doi:10.19762/j.cnki.dizhixuebao.2011.01.001

Yang, W. X., Yan, D. P., Qiu, L., Wells, M. L., Dong, J. M., Gao, T., et al. (2021). Formation and forward propagation of the indosinian foreland fold-thrust belt and nanpanjiang foreland basin in SW China. *Tectonics* 40, e2020TC006552. doi:10.1029/2020TC006552

Ye, T., Chen, X., Liu, Z., Wang, P., Dong, Z., Cui, T., et al. (2022). A magnetotelluric study of 3D electrical resistivity structure underneath the southern

segment of the Red River Fault zone, South China. *J. Asian earth Sci.* 225, 105056. doi:10.1016/j.jseaes.2021.105056

Yin, A., and Harrison, T. M. (2000). Geologic evolution of the himalayan-Tibetan orogen. *Annu. Rev. Earth Planet. Sci.* 28, 211–280. doi:10.1146/annurev.earth.28.1.211

Yu, H., Hu, F., Xu, J., Zhang, Z., and Chen, X. (2022). Dynamic rupture simulation of the 1833 Songming, Yunnan, China, *M* 8.0 earthquake: effects from step over location and overlap distance. *Earth Space Sci.* 9, e2021EA002100. doi:10.1029/2021EA002100

Yunnan Bureau of Geology and Mineral Resources (1990). *Regional geological records of Yunnan Province*. Beijing: Geological Publishing House.

Zhang, E., Lou, H., Jia, S., and Li, Y. (2013). The deep crust characteristics beneath western Yunnan. *Chin. J. Geophy.* 56, 1915–1927. doi:10.6038/cjg20130614

Zhang, H., Zhang, P., Wu, Q., and Chen, Z. (2008). Characteristics of the Huanghe river longitudinal profiles around Xunhua-Guide area (NE Tibet) and their tectonic significance. *Quat. Sci.* 28, 299–309. doi:10.3321/j.issn:1001-7410.2008.02.012

Zhang, J., and Ding, Z. (2016). Discussion about several issues on dien bien Phu Fault and north–south seismic belt. *J. Seismol. Res.* 39, 527–536. doi:10.3969/j.issn.1000-0666.2016.04.001

Zhang, J., Zhong, D., Sang, H., and Zhou, Y. (2006). Strucyural and geochronological evidence for multiple episodes of deformation since Paleocene along the Ailao Shan-Red River shear zone, Southeastern Asia. *Chin. J. Geoolgy* 41 (2), 291–310. doi:10.3321/j.issn:0563-5020.2006.02.011

Zhang, P., Deng, Q., Zhang, G., Ma, J., Gan, W., Min, W., et al. (2003). Active tectonic blocks and strong earthquakes in the continent of China. *Sci. China Ser. D. Earth Sci.* 46, 13–24. doi:10.1360/03dz0002

Zhang, Y., Yan, D. P., Qiu, L., Gong, L., and Shao, Y. (2023). Stepwise growth of the southeastern Tibetan Plateau: structural and thermochronological evidence from the Panxi tectonic belt. *Palaeogeogr. Palaeoclimatol. Palaeoecol.* 621, 111542. doi:10.1016/j.palaeo.2023.111542

Zhao, X., Zhang, H., Lease, R. O., Wang, Y., Pang, J., Li, Y., et al. (2023). Early Cenozoic drainage evolution and surface uplift of the eastern Tibetan plateau: insights from the Ninglang basin. *Geophys. Res. Lett.* 50, e2023GL105499. doi:10.1029/2023GL105499

Zhou, Q., Li, X., Chang, Y., Yu, J., Luo, W., and Bai, X. (2023). Strong earthquake recurrence interval in the southern segment of the Red River Fault, southwestern China. *Front. Earth Sci.* 11, 1280787. doi:10.3389/feart.2023.1280787